Experimental Thermal and Fluid Science 146 (2023) 110920

Contents lists available at ScienceDirect

Experimental Thermal and Fluid Science

journal homepage: www.elsevier.com/locate/etfs

Insights from sloshing experiments in a rectangular hydrophobic tank

Fatih C. Korkmaz [a,*], Bülent Güzel [b]

[a] Department of Marine Engineering, Yildiz Technical University, Istanbul, Turkey
[b] Department of Mechatronics Engineering, Istanbul Gelisim University, Istanbul, Turkey

ARTICLE INFO

Keywords:
Sloshing
Hydrophobic coating
Pressure measurement
Free surface deformation

ABSTRACT

The wave impingement on the side walls due to the oscillation of a rectangular tank under harmonic sway motion is analysed experimentally with hydrophobic coated and uncoated tank surfaces. Impact pressures and free surface deformations are compared in three water filling levels over an excitation frequency range encompassing the first natural frequency. The reduced hydrodynamic loads acting on the tank walls are observed under hydrophobic effects and discussed in detail. Experimental observations clearly indicate that there is a strong effect of the solid surface properties on the free surface elevation, wave generation and pressure distribution. In particular, major changes have been traced around the resonance frequency due to more dominant tangential flow and altered wave form, which results in lower peak pressure values with increased water movement within the tank under the hydrophobic effects.

1. Introduction

Sloshing is a violent liquid motion experienced in partially filled liquid tanks which can be observed in many different engineering applications e.g. oil tankers, space shuttles. It has gained a particular attention in ocean engineering since sloshing induced impact loads may affect the stability and operating conditions of liquid carrying ships, the structural characteristics of liquid tanks and their orientation in a ship. These loads may become very large in magnitude and damage the liquid tank walls in a ship when the frequency of sloshing is near the natural frequency of the ship. The suppression of these large amplitude motions due to the excitation from external forces is one of the main concerns for design engineers.

Sloshing under the sway excitation in a partially filled tank is a free surface flow between the tank walls that can generate high wave impacts on the side walls. Therefore, investigating the sloshing phenomenon is mostly associated with the mechanism of wave generation, wave types and the impact pressures acting on the tank walls. The wave form may change with the magnitude and the frequency of the excitation, filling level and the tank length, resulting in altered impact characteristics. Ibrahim [8] provides a comprehensive review on breaking waves and liquid sloshing impacting on rigid walls and in liquid containers. Theoretical methods for sloshing in various geometries was discussed in detail along with the compilation of the results obtained experimentally and numerically. The effect of aeration and air compressibility during sloshing is studied by Peregrine and Thais [25]. Cuomo et al., [4] studied the breaking wave impacts on coastal structures. Bredmose et al. [2] studied the aeration effect in various types of wave impacts using analytical and numerical methods. They reported a reduction in the impact loads acting on the structure due to aeration in all types of wave loading. Karimi et al. [14] identified different wave geometries during sloshing at three different gas–liquid density ratios and discussed their effects in a chamfered tank. Zou et al. [41] carried out experiments to investigate the effects of liquid viscosity on sloshing under roll excitations, and reported that the impact pressures on walls decrease with increasing viscosity, while the rising times increase. Jin and Lin, [10] experimentally and numerically investigated the effects of viscosity on liquid sloshing under external excitations using the large-eddy-simulation (LES) for turbulent effects. They concluded that the maximal wall pressure decreases with increasing viscosity, and the high viscosity liquid is adhered onto four side walls. Watanabe et al. [32] simulated the sloshing waves at shallow depth conditions with flat and sloped bottoms. Wu et al. [35] studied sloshing in a tank excited at three lowest natural frequencies at the low filling case under coupled rolling and pitching motions. They concluded that violent sloshing motion occurred at the lowest natural frequency of the tank, and some other extensive impacts are generated on the roof of tank. Luo et al., [20] experimentally investigated the 3D sloshing in a membrane-type LNG tank under combined roll and pitch excitations. They classified the sloshing waves into four patterns: the length-dominant wave, swirling

* Corresponding author at: Yildiz Technical University, Istanbul 34349, Turkey.
E-mail address: fkorkmaz@yildiz.edu.tr (F.C. Korkmaz).

https://doi.org/10.1016/j.expthermflusci.2023.110920
Received 19 September 2022; Received in revised form 11 March 2023; Accepted 2 April 2023
Available online 5 April 2023

wave, diagonal wave, and breadth-dominant wave with the swirling wave inducing intensive impact pressures on the walls and being the most observed one. Gurusamy et al. [5] reported that the hydraulic jump is observed when the excitation and natural frequencies meet.

Minimizing the sloshing induced loads has been the focus in numerous research studies. Since damping due to the liquid viscosity is insufficient, in order to minimise motion over a range of frequencies, various suppression methods have been suggested. Installing solid/perforated baffles vertically or horizontally or keeping them a float in liquid tanks are the most common practices to mitigate sloshing-induced flows and dissipate the sloshing energy (Faltinsen and Timokha, 2011, Molin and Remy [22,9,37,1]. Baffles can also significantly shift the natural frequency of a liquid carrying tank and suppress the free surface deformations at varying rates (Wei et al. [33], Faltinsen and Timokha [45], 2011, [26], Korkmaz and Guzel [17], Jin et al. [11]). Yu et al. [38] studied the harmonic roll excitation in LNG shaped tanks to test floating devices in supressing the sloshing. Different tank shapes are considered as well in reducing the sloshing loads. Zhang et al. [39] numerically investigated the effect of wedge shaped tanks in preventing sloshing induced instabilities in ship motions. Sauret et al. [42] proposed to place foams on the free surface of the liquid to suppress the sloshing. Zhang et al. [40] conducted experiments and considered various floating foams placed on the free surface to limit the sloshing motion. Korkmaz [16] showed that top-layer high viscous liquids could dissipate sloshing of bottom-layer low viscous liquids.

Suggested sloshing suppressing methods introduce either extra solid material/structure which increases the weight of ships and interferes with loading/unloading and cleaning processes, or liquid material which may interact with the ship load and require extra processes for removal. The sloshing loads and natural frequencies are independent of the liquid viscosity, but their dependency on contact angle and surface tension has not been explored. The effect of the wettability of the tank surface in sloshing has never been investigated. It is considered that altering the solid surface characteristics on tank walls may yield another option, without using baffles/screens or different tank shapes, in mitigating the sloshing loads. In this regard, using hydrophobic surfaces in various liquid–solid interaction applications already give some interesting and promising results in changing the flow dynamics [31,6]. Hydrophobic surfaces create a contact angle more than 90° for a free liquid droplet with solid surface. In such a decreased wetting state, liquid particles sit on a mixture of solid and air resulting in less contact area between the solid surface and the liquid. Hydrophobic surfaces may reduce the drag due to the slippage created on solid surfaces in various types of flows e.g. pipe flows, Taylor-Couette flows. The effect of hydrophobicity on flow characteristics has been demonstrated in water-entry studies of various geometries i.e. modifying macroscale hydrodynamics [27,28,7]. In these studies, a reduction in the impact loads has been observed when using hydrophobic surfaces.

Collision dynamics of a small water droplet on a solid surface can be altered significantly by changing the wettability characteristics of the solid surface as well [31]. Drop deformation depend strongly on surface properties. On hydrophobic surfaces, water droplets may move freely or even bounce during interactions with solids. The contact angle may play an important role on the balance of kinetic, surface and potential (gravitational) energies during the bouncing of a water droplet. In general, sloshing is characterized by free surface deformations and impact loads on the side walls depending on the liquid filling levels and excitation frequencies. The surface properties of a solid structure may influence the wave impact [24]. Evolution of waves, water climb-ups and the impact pressures acting on side walls during sloshing phenomenon when hydrophobic effects are present have never been investigated. Since hydrophobic effects induce droplet collisions to be more elastic, hydrophobicity can cause reduction in the impact pressures during sloshing, which may lead to eliminating or minimizing the usage of baffles in suppressing the sloshing loads without adding extra weights or shifting the natural frequency. In this paper, the hydrodynamic aspects of liquid sloshing under hydrophobic effects in a sway-oscillated rectangular tank have been examined. For this purpose, various filling levels and oscillation frequencies are considered. First, the fluid response, wave elevations and free surface deformations have been compared for uncoated and hydrophobic coated surfaces when subject to sinusoidal excitation. Then, pressure measurements have been carried out for both cases in the present study.

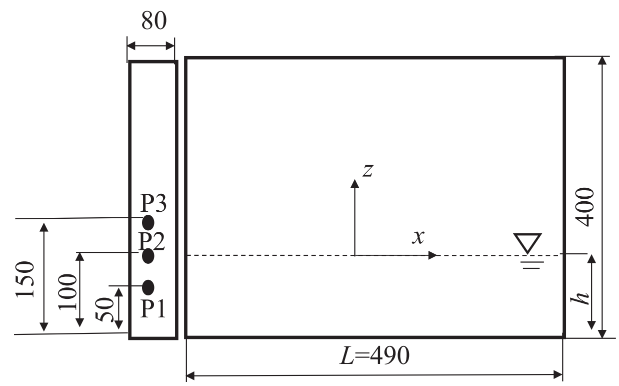

Fig. 1. Sketch of the test tank and pressure sensor locations. Dimensions in mm.

2. Experimental setup

An experimental setup is designed and constructed to observe two-dimensional liquid sloshing in a rectangular tank (Fig. 1). The tank is made of plexiglass with the dimensions of 490 × 400 × 80 mm. In order to conduct the experiments under the same test conditions, the tank is mounted on a low-friction linear motion table and forced to oscillate horizontally with an amplitude of 110 mm at various frequencies. Single amplitude is chosen since the excitation amplitude has a minimal influence on the frequency of the sloshing phenomenon and free surface elevation. One degree of freedom monoharmonic periodic motions of the tank are controlled by an induction motor (220 V AC, 1 phase) with frequency inverter resulting in a 2D response. Throughout the manuscript, the three filling levels (h), 50, 100, 150 mm are named as low, medium and high filling level, respectively. The free surface elevation and impact pressure are investigated with uncoated and hydrophobic coated surfaces.

The filling level, the excitation frequency and the natural frequency of the tank are important parameters in sloshing phenomenon. The natural frequency of the tank depends on the filling level and the length of tank and is determined according to linear theory as:

$$\omega_n = \sqrt{g\frac{n\pi}{L}\tanh\left(\frac{n\pi}{L}h\right)} \tag{1}$$

Where L is the tank length, h is the water filling level, g gravity and n is the mode number. The resonance condition cannot be obtained directly through this formulation due to the non-linearity of the sloshing problem when taking the mode number one. However, resonance frequencies are close to the values obtained with this formulation. The natural frequencies, ω_1 in the low, medium and high filled cases are calculated as 4.41 rad/s, 5.96 rad/s and 6.84 rad/s respectively. First, sixteen oscillation frequencies ranging between 2.8 and 7.3 rad/s which include the smallest natural frequencies for the test tank are studied with uncoated surfaces. Then the same experiments are carried out with hydrophobic coated surfaces.

Phantom Miro eX4 model high speed camera is used to capture wave elevations and free surface deformations. The water is dyed with blue food colouring for better optical detection in the hydrophobic case. The high-speed camera is focused on the centre plane of the rectangular tank to catch the free surface movements. The high-speed images are

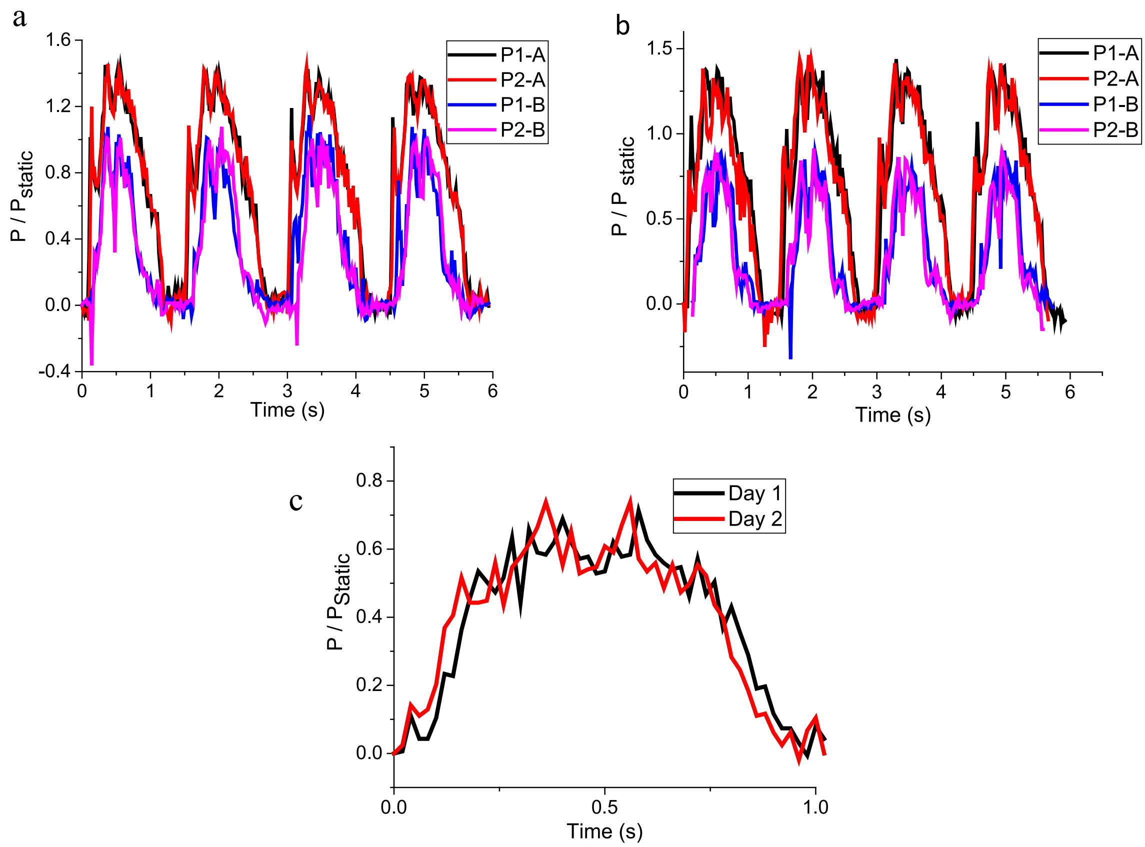

Fig. 2. Repeatability of the sloshing tests in the medium filling level at 0.69 ω/ω_n with (a) uncoated and (b) hydrophobic coated surface. P1 and P2 are positioned at 50 mm (A) and 100 mm (B) from the bottom. (c) P2 measurements in two different days at 0.56 ω/ω_n excitation.

acquired at 500 fps. An LED lighting panel is placed in the background of the tank to ensure the brightness and clarity of the images. The dynamic pressure acting on the side wall is measured by three water-tight pressure sensors (SHLLJ-PCM300D) ranged between 0 and 0.4 bar and placed at 50 mm interval from the bottom. HIOKI LR-8500 model DAQ system is used to collect the pressure signals at a sampling frequency of 200 Hz. Although larger sampling frequency values are recommended for capturing the maximum peak pressure values ([15], Luo et al. [20]), Jin et al. [12] stated that lower sampling frequencies are good enough in capturing the general features of the impact process if the rising time is not of concern. Before carrying out the experiments, the pressure transducers were switched between the measuring points to demonstrate repeatability. Fig. 2a shows pressure–time histories at two measurement points obtained with two different pressure transducers (P1 and P2) on the wall under non-resonance oscillation frequencies. Pressure measurements in each test condition was carried out for 80 corresponding cycles of excitation in order to ensure the steady state dynamic conditions, and the first 30 cycles were neglected.

Hydrophobic surface is created by applying a chemical coating by Wetproof Inc. creating a micro scale roughness on the test tank surface without changing the dimensions and the mass of the tank. Measurements of the contact angle in the equilibrium state were taken using the Theta optical tensiometer from Attention. The measured contact angles vary between 148 and 160° on the hydrophobic coated surface, which confirms an apparent angle of around 150° that shows clear evidence of superhydrophobic behavior on the coated surfaces. During the contact angle measurements, it was observed that the water droplets roll off the hydrophobic coated surface when it is tilted with an angle as small as 3°. This small contact angle hysteresis shows that the dynamic contact angle is not much different from the static one, which confirms wetting in the Cassie–Baxter state. When a water droplet hits on a solid surface, the outcome following impact may be evinced to three different forms, depending on the surface characteristics and the Weber number ($We = \rho V_0^2 R/\sigma$ where ρ is the density, V_0 is velocity, R is the radius of the droplet and σ is the surface tension); spreading, rebounding, splashing [36]. In order to visualize such an impact under hydrophobic effects created by the chemical coating in this study, a water droplet is released from 5 cm height ($We = 8$–12) to free fall onto the uncoated and

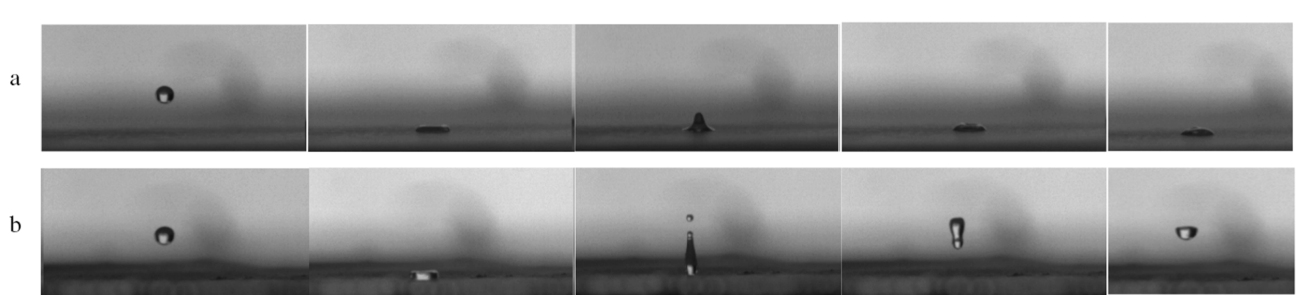

Fig. 3. Free fall of a water droplet from 50 mm on uncoated [a] and hydrophobic coated surfaces [b.]

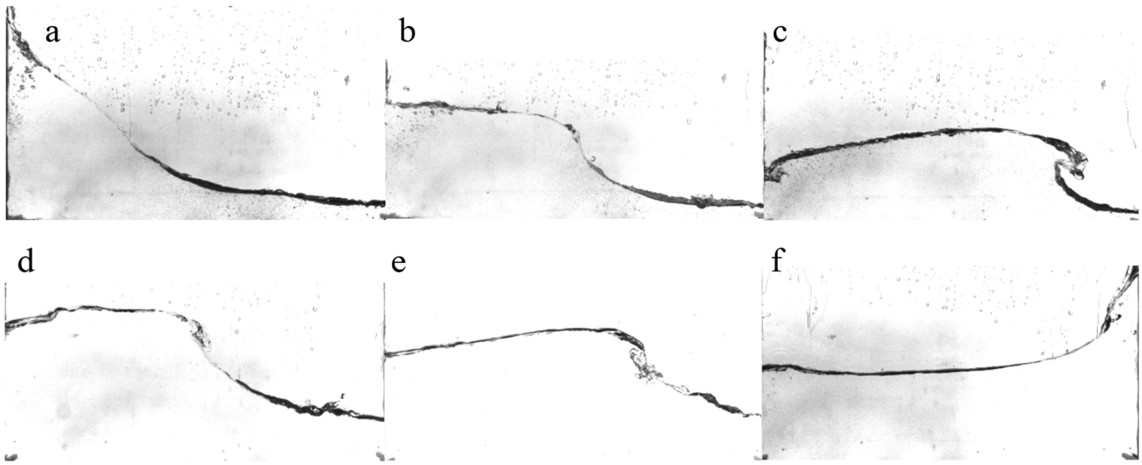

Fig. 4. Medium [a, b, c] and high [d, e, f] filling levels at 0.87 ω/ω_n and 0.76 ω/ω_n (125 ms [a, d],200 ms [b, e], 300 ms [c, f]).

hydrophobic coated surfaces as seen in Fig. 3. On the uncoated surface, the water droplet sticks to the solid surface (Fig. 3a). Whereas the impact becomes more elastic on the hydrophobic coated surface due to having lesser contact area with water, and the water droplet bounces back in the air i.e. separating from the solid surface (Fig. 3b). In both cases, first, the droplet shrinks vertically and spreads laterally increasing the surface area of the droplet after the impact converting the kinetic energy of the droplet to the surface energy. While the energy is dispersed and completely transferred to the solid surface in the uncoated case (Fig. 3a), the increased surface energy cannot overcome the surface tension, and the droplet acts like an elastic ball with some energy stored within in the hydrophobic case (Fig. 3b). Having less drag and more elastic collision, it can be expected that energy balance during sloshing impacts may change significantly under hydrophobic effects.

3. Results and discussion

In this section, the experimental results obtained in three filling levels under the effect of various excitation frequencies are presented for 2D monoharmonic uncoated and hydrophobic coated cases in order to gain some insight into sloshing loads under hydrophobic effects. The wave run-up, free surface elevation and pressure measurements on the side wall are generally considered as the most significant characteristics for comparison of the impact loads, local and global effects in liquid sloshing. Another phenomenon to be observed in a sloshing event is air entrapment. As the waves propagate to the other side of the tank, an air cavity trapped by an overturning wave crest may be observed. Then, this entrapped air in the wave crest disintegrates into bubbles after the wave hits the sidewall. During this stage, the flow becomes aeriated due to collapsing of the air bubbles, which may affect the impact characteristics (Wood, [34]). The level of aeration can increase the duration of an impact i.e. higher pressure and forces acting on the wall [34,19,3]. On the other hand, some studies reported that the entrapped air may lead to air cushioning effect [25,24,2]. Before taking into account the hydrophobic effects, qualitative analysis of sloshing flow in the experimental setup is performed using a high-speed camera in Section 3.1 and carrying pressure measurements in Section 3.2. The wave run-up along the side wall is associated with the global loads of sloshing, which affect the ship motions. The impact pressure on the side walls is associated with the local loads of sloshing, which affect the tank structure.

3.1. The free surface deformation

Excitation frequency, excitation amplitude and water depth are three main parameters affecting the free surface deformations [29]. The type of wave is determined by the vertical and horizontal wave velocity differences [44]. When the horizontal velocity is greater than the vertical one, a breaking wave is formed. When vice versa, it forms a wave in the process of breaking. A standing wave occurs when the horizontal wave velocity is too large. These differences in wave types affect the magnitude of the impact pressure. The impact pressure is maximum around the still free surface level in case of the standing and breaking waves (Kortenhaus et al. [43]). A larger amount of energy of the wave is used up during the first stages of the impact, then the remaining energy is spent for the rise-up on the sidewalls. Therefore, pressure magnitude towards the roof of the tank is decreased. Fig. 4 shows the free surface

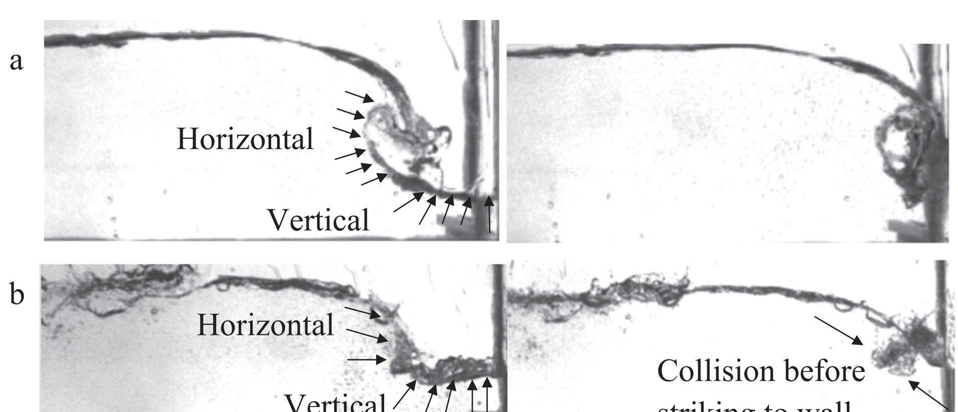

Fig. 5. The effect of oscillation frequency in the medium filling level at 0.87 [a] and 1.05[b] ω/ω_n.

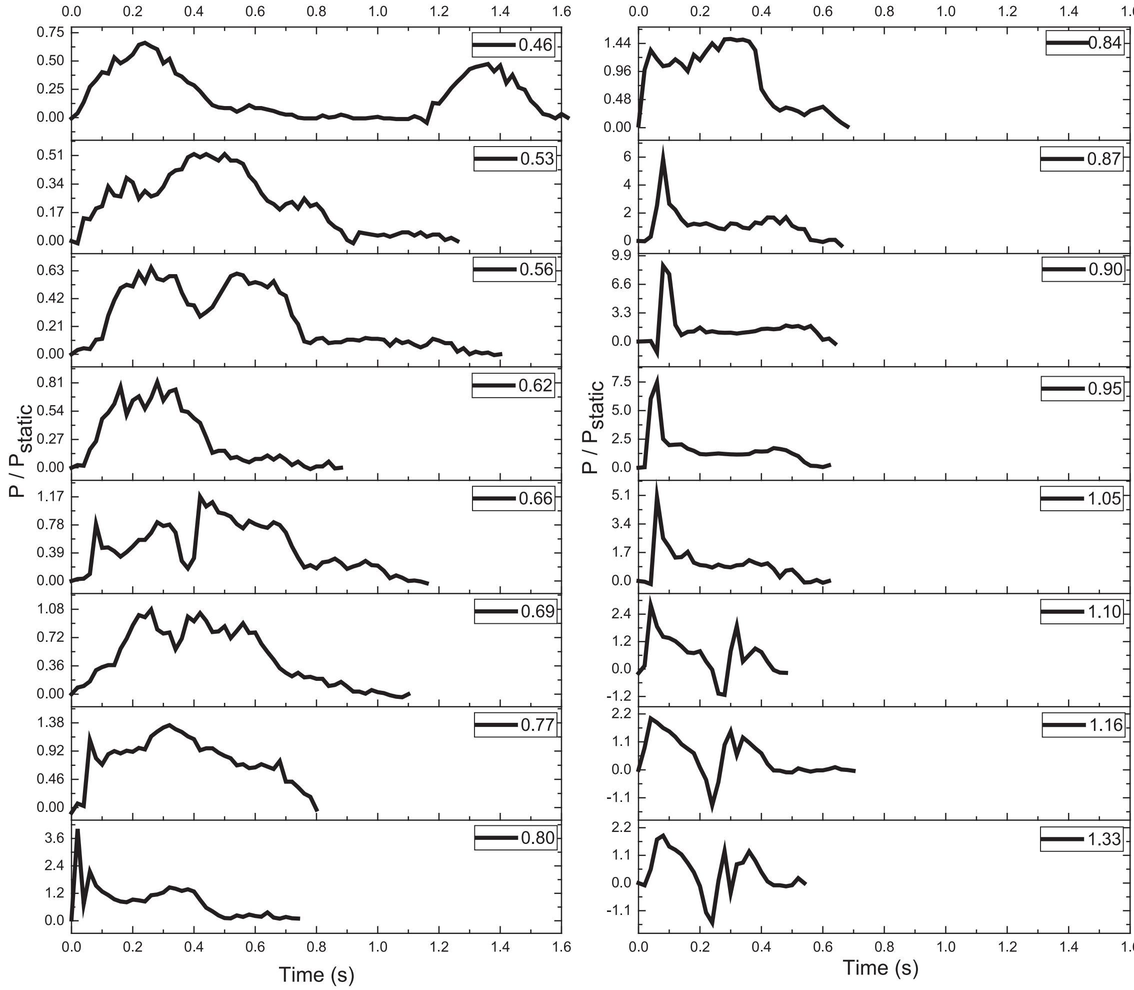

Fig. 6. The pressure–time histories at P2 under various frequencies in the medium filling level.

elevations and the wave propagation in the medium and high filling levels at $\omega/\omega_n = 0.87$ and 0.76 oscillation rates, respectively in the uncoated case. The behaviour of the bulk water changes with the filling level i.e. higher run-up occurs and the wave forms 100 ms later in the medium filling level (Fig. 4a, b). The progressive wave breaks near the vertical wall in the medium filling level (Fig. 4c). However, a non-breaking wave propagates through the tank until hitting the sidewall in the high filling level (Fig. 4e, f).

Depending on the filling level, sloshing may produce different flow phenomena. Excitation frequency is another significant parameter which can alter the wave and impact characteristics on the side wall. Fig. 5 shows the wave collision on the sidewall at two different excitation frequencies in the medium filling level. The horizontal velocity of the wave dominates before the impact in both cases. The vertical and horizontal components of the excited water merge together before the impact at the higher oscillation level (Fig. 5b). The hammer shock impact with massive force is blocked from hitting the wall directly due to the risen water vertically near the side wall. The wave crest collides with the vertical risen water i.e. dampening some part of the wave energy before the impact. However, at the smaller oscillation frequency, the vertical component of the wave velocity is overcome by the horizontal component, then, the hammer shock pressure takes effect where the wave crest strikes the sidewall (Fig. 5a).

3.2. *The pressure distribution on sidewalls*

The impact pressures on the side walls during sloshing are repetitive with random magnitude values and localized in space and time. The magnitude of pressure on the side walls depends on the excitation frequency and filling level. Fig. 6 shows the pressure–time histories obtained under 16 excitation frequencies in the medium filling level for the uncoated case. The pressure values are normalized by the static pressure in the calm water i.e. ρgh. The pressure builds up gradually at lower frequencies. At near-resonance frequencies, sharper peak pressure values are observed due to larger wave nonlinearities (Fig. 7b,c), therefore the fluid carries more energy. In the vicinity of the resonance frequencies (0.87 to 1.16 ω/ω_n), two peaks of pressure are observed, the first one is as much greater than the second one (Fig. 6). However, smaller free surface deformations and pressure values are observed at the lower frequencies (Fig. 7a).

Fig. 7. Snapshots of the impact taken in the medium filling level at 0.77 [a], 0.87[b] and 1.05[c] ω/ω_n.

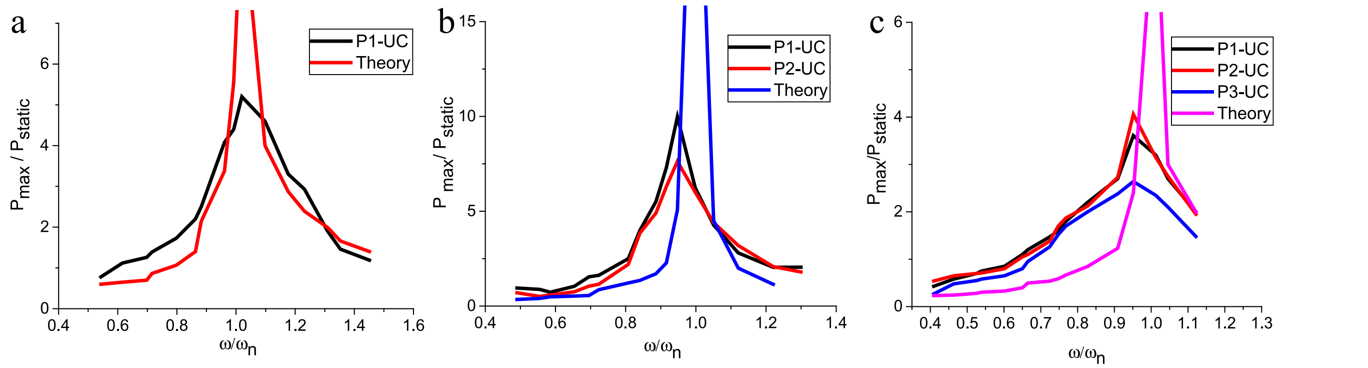

Fig. 8. The peak pressure values vs. excitation frequencies in low [a], medium [b] and high [c] filling levels.

Other than the peak pressure, duration of the impact is another parameter that affects the structural deflection, and may be dominant on the structural damage [3]. Therefore, low oscillation frequencies still need to be taken into account just as much as the near-resonance frequencies in the design considerations. The side wall is subject to the sloshing pressure for 0.5 s in one cycle at the higher oscillation

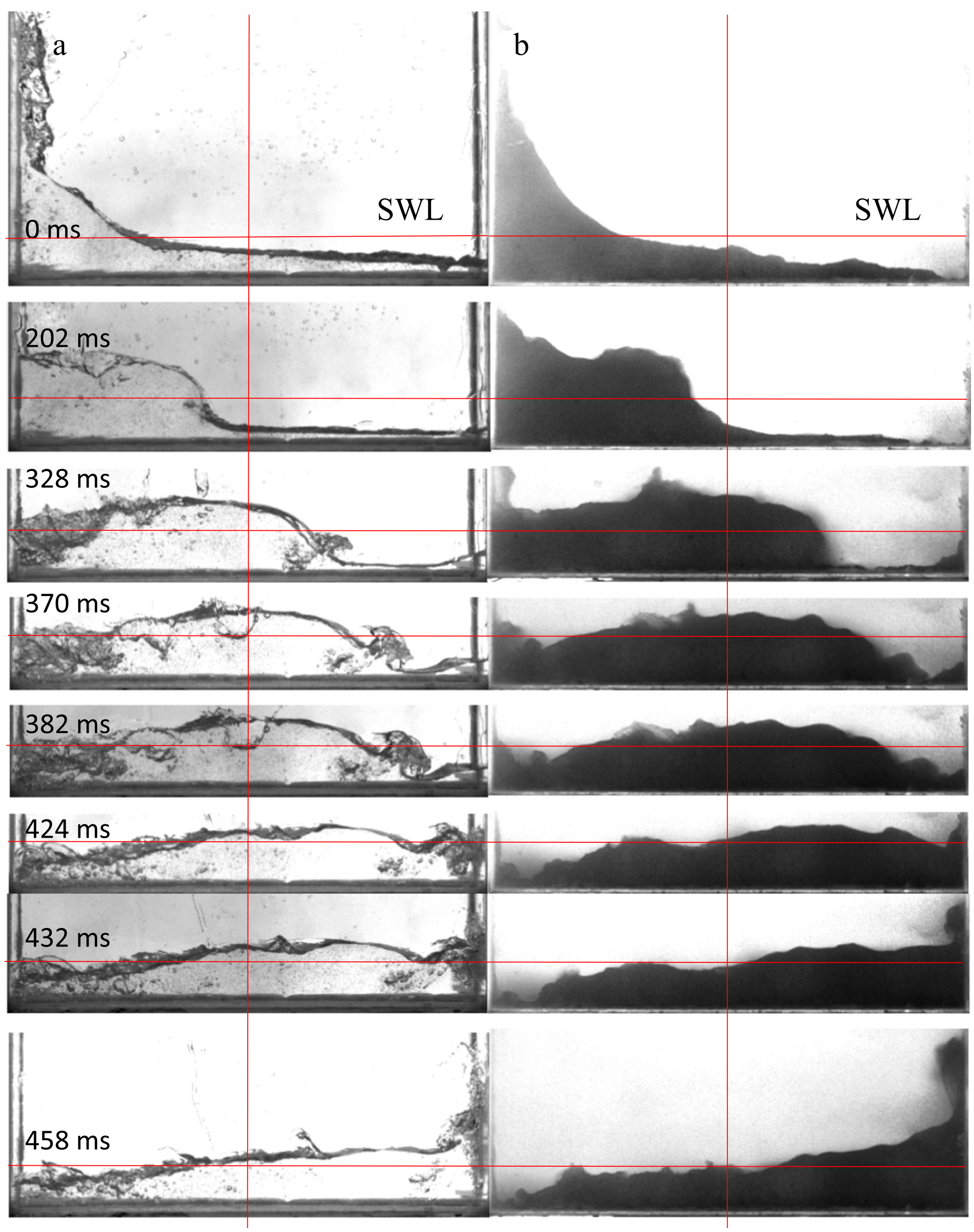

Fig. 9. Snapshots taken at 1.17 ω/ω_n excitation in the low filling level (UC [a] and HC [b]).

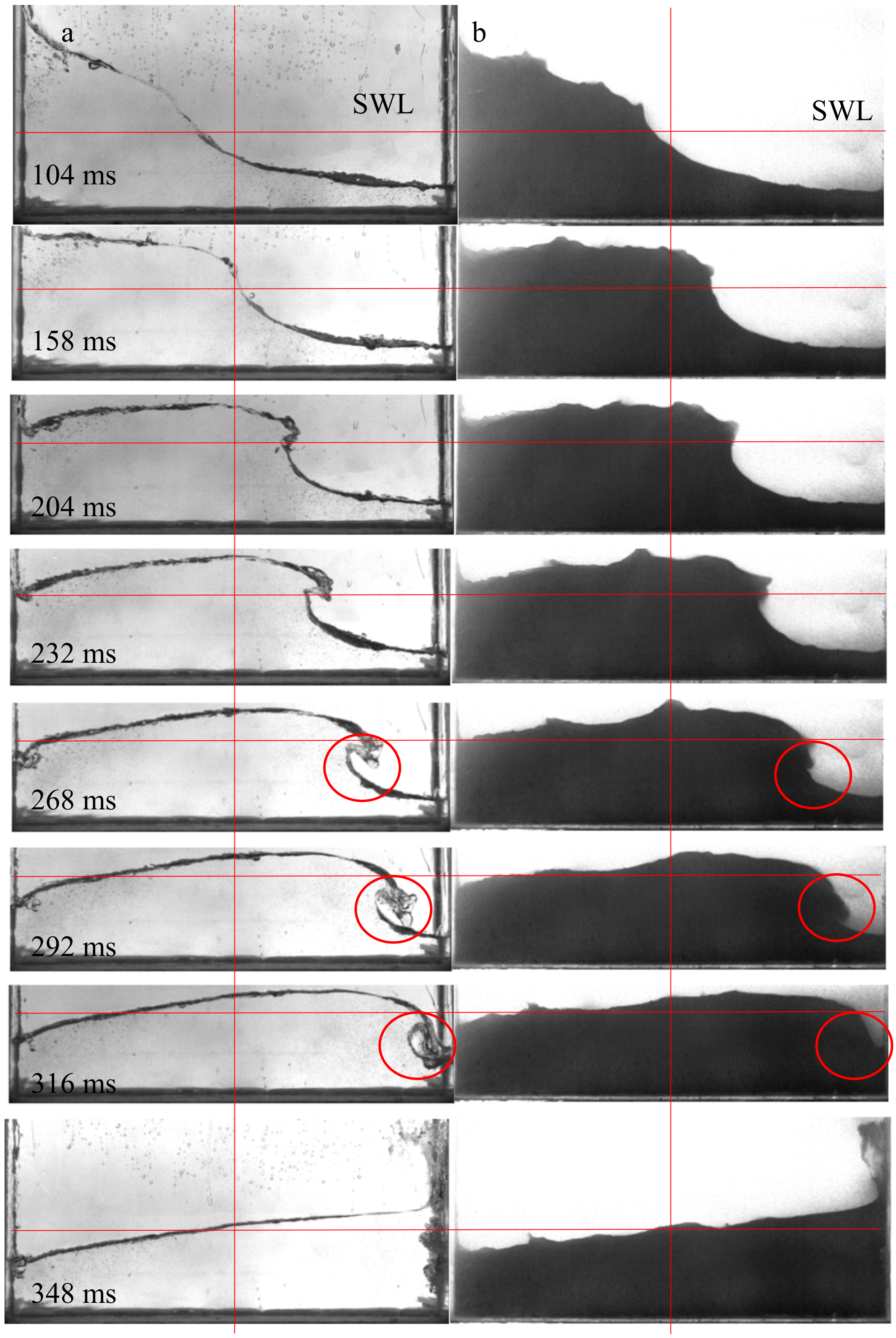

Fig. 10. Snapshots taken at 0.87 ω/ω_n in the medium filling level (UC [a] and HC [b]).

frequencies, whereas their duration is tripled at the lower oscillation frequencies (Fig. 6).

In order to compare the average peak pressure values with respect to the excitation frequencies varying from 0.54 to 1.45 ω/ω_n in the low filling level, 0.4 to 1.22 ω/ω_n in the medium filling level and 0.4 to 1.1 ω/ω_n in the high filling level, normalized peak pressure values versus normalized excitation frequency values are plotted in Fig. 8. The peak pressure increases and takes maximum values at the near-resonance frequencies, and it has much lower values in the off-resonance regions. Fig. 8 also compares the experimental measurements with the theoretical results obtained from the following formulation [13],

$$P = \rho\left[\sum_{n=0}^{\infty} \mathrm{sin}k_n x\mathrm{cosh}k_n(z+h)[-E_n\omega_n sin\omega_n t - F_n\omega\mathrm{sin}\omega t] - \frac{1}{g}A\omega x sin\omega t\right] \tag{2}$$

Where ρ is density, $k_n = \frac{2n+1}{L}\pi$, $F_n = \frac{\omega D_n}{{\omega_n}^2-\omega^2}$, $E_n = -F_n - \frac{D_n}{\omega}$, $D_n = \frac{4\omega A(-1)^n}{Lcosh(k_n h)}\frac{1}{{k_n}^2}$.

The discrepancy between the experimental results and the

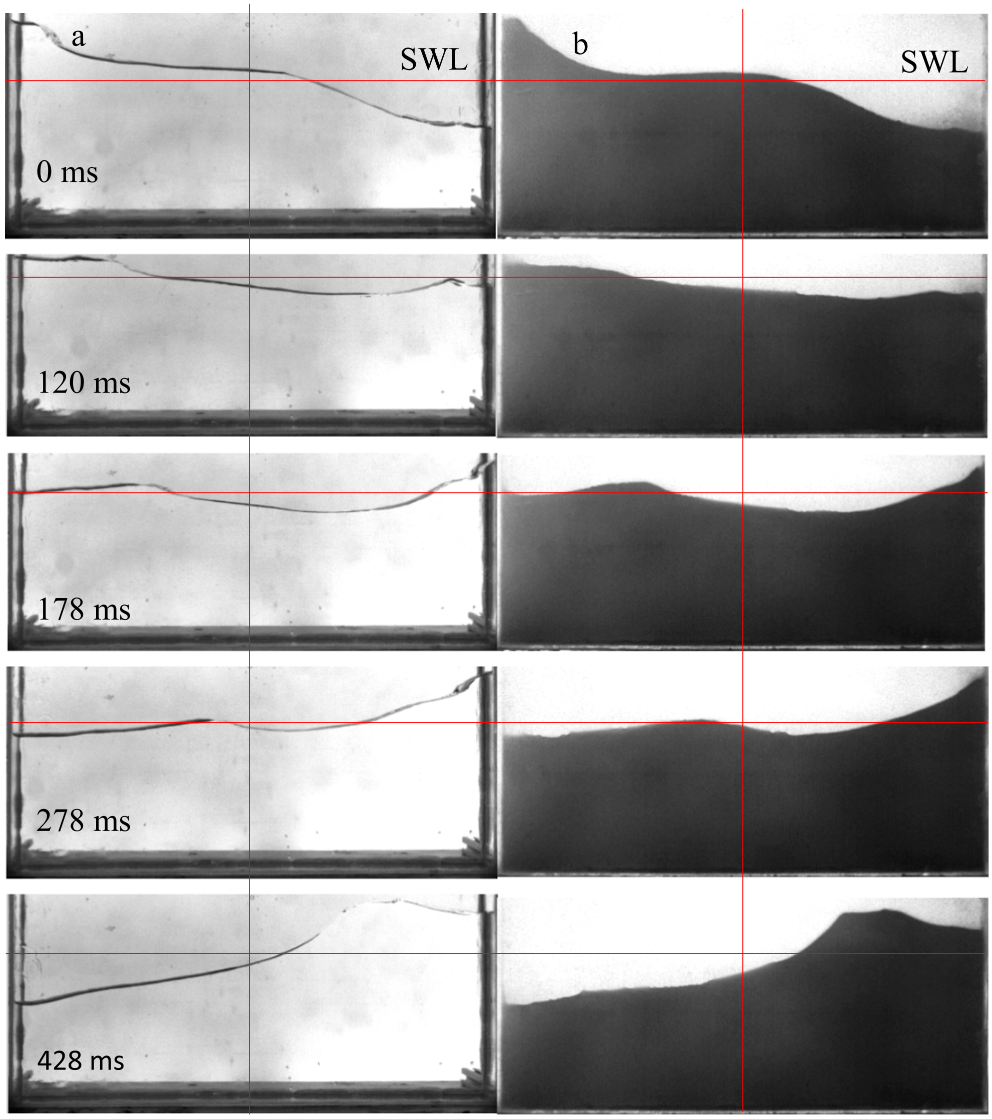

Fig. 11. Snapshots taken at 0.65 ω/ω_n in the high filling level (UC [a] and HC [b]).

theoretical values in the first mode natural frequencies in Fig. 8 may be associated with the nonlinear free surface effects and the wall friction which are not considered in the theory. It can also be noticed in Fig. 8 that the corresponding peak pressure values have similar trends as in the free surface elevations. It should be noted that the integration of the local pressure over the side wall may have higher total sloshing-induced forces acting on the wall in the high filling level despite the lower peak values.

3.3. The effect of hydrophobicity on free surface deformation

Other than liquid viscosity, excitation frequency and filling level, the roughness of solid surface or sloping and curving in the tank geometry are some other parameters that affect the impact characteristics [24]. In this section, the experiments conducted under hydrophobic effects are presented. In numerical simulations, hydrophobic and hydrophilic surfaces are modelled with respectively free-slip and no-slip body boundary conditions in the literature. Similarly, for the potential or rotational inviscid flows, the condition for the non-porous walls is generally the free-slip (Newmann) condition [10,21]. Luo et al. [21] provides an extensive review on particle-based Lagrangian mesh free simulations of wave generation, propagation, breaking and air entrainment. Jin and Lin, [10] reported that their numerical results with free-slip velocity boundary condition overestimated pressure amplitude compared to the no-slip results and the measured data. They also stated that the free-slip results are also ahead of the measured data in phase. It is also known that hydrophobic surfaces may reduce the drag due to the slippage created on solid surfaces. Figs. 9-10 compare the free surface elevations under the same excitation frequency in the low and medium filling levels, respectively for the uncoated (UC) and hydrophobic coated (HC) cases. The horizontal red lines in Figs. 9-10 represent the still water line (SWL), and the vertical ones divide the tank into halves for comparison. Different characteristics of wave run-ups, free surface elevations and wave propagations are observed in the hydrophobic cases. The wave and the bulk water moves faster in the hydrophobic case due to reduced drag, and the wave front always stands in a further position at each time instant. This means that the rising times decreases as similarly seen in a low viscosity case. In the low filling level, more violent and chaotic fluid transfer with broken free surface and generation of massive droplets is observed in both cases (Fig. 9). At the beginning and the end of the recorded cycle in Fig. 9 e.g. at 0, 202, 432 and 458 ms, it is seen that some amount of water always remain at the tank bottom in the uncoated case. Whereas, the tank bottom dries up in the hydrophobic case i.e. more water is displaced due to reduced drag under hydrophobic effects. This indicates that the free surface elevations in the hydrophobic case are ahead of the ones in the uncoated case in phase. In the medium

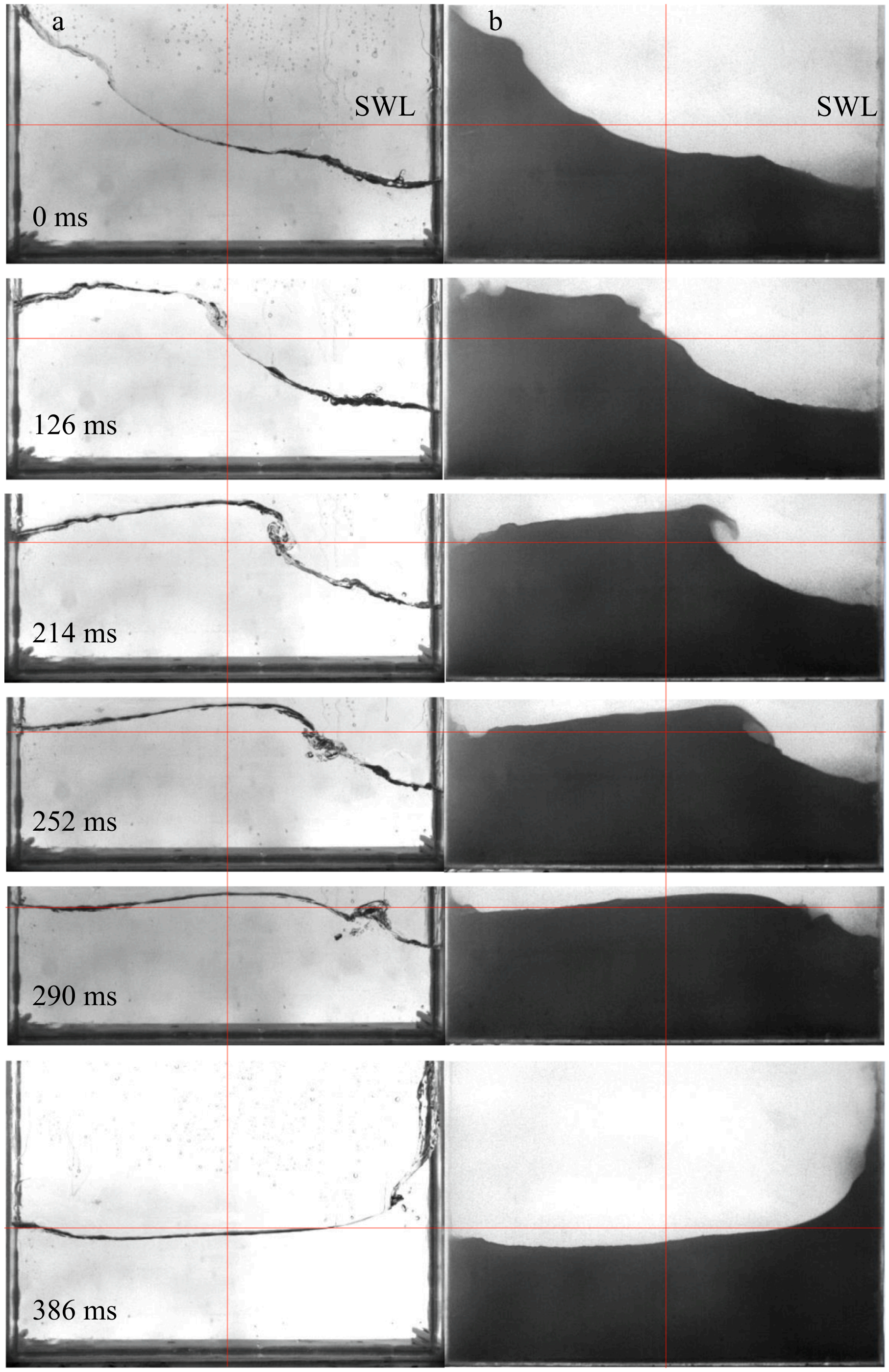

Fig. 12. Snapshots taken at 0.76 ω/ω$_n$ in the high filling level (UC [a] and HC [b]).

filling level, wave evolution have different characteristics in the hydrophobic case as well. The horizontal component of the wave velocity surpasses the vertical component at the bottom of the wave crest in the uncoated case, so it takes the shape of a concave (Fig. 10). This velocity difference is increased near the sidewall, then the wave crest overturns. The air is trapped under the wave crest, then the wave hits the sidewall with entrapped air (Fig. 10 at 316 ms). In this case, the impact is defined as compression shock [4]. Due to the air pocket, the aerated impact occurs. Due to collapsing of the entrapped air and the ejection of water, jet flow rises to the top of the tank with a booming sound [23]. However hydrophobic surface changes the tangential flows, the wave crest splits, therefore wave forms without an air cavity i.e. the air can escape at bottom of the wave crest. As a result, the wave without air hits the sidewall and this type of impact is called ventilated shock [4].

The wave impact with air bubbles can change the structural response of a tank [18], especially at the resonance frequency. However, under hydrophobic effects, the wave tip follows a trajectory without air bubbles, therefore, the impact history on the side wall is hydrodynamically and structurally different from the one with the uncoated surface. Topliss [30] estimated the air bubble cavitation frequency (f_r) for a 2D cavitation occurring within a free surface region as follows:

$$f_r^2 = -\frac{2\gamma p}{4\pi^2 \rho r^2 \log\left(\frac{r}{2h_y}\right)} \tag{3}$$

where p is atmospheric pressure, γ is the specific heat ratio, r is the

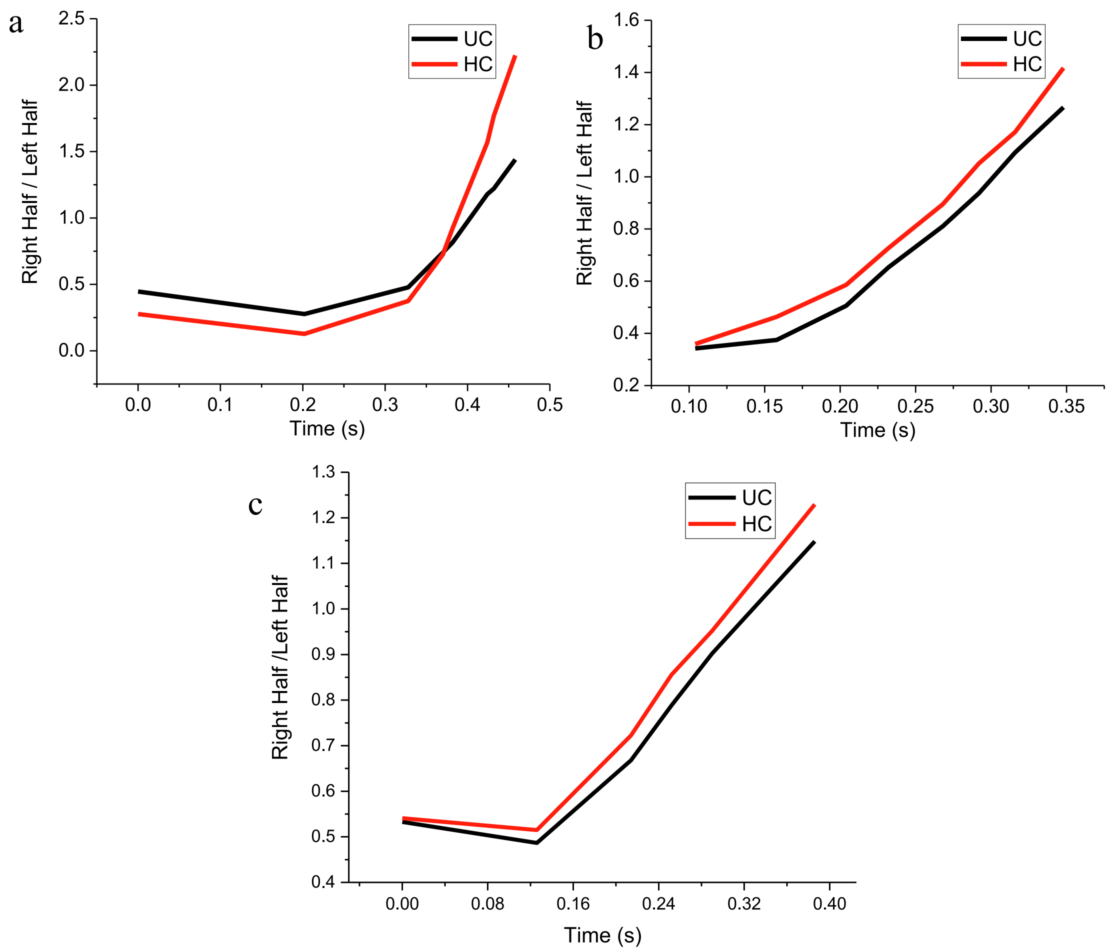

Fig. 13. The water ratio between two vertical halves of the tank during one cycle in the low filling level [a], the medium filling level [b] and the high filling level [c] at 1.17, 0.87 and 0.76 ω/ω_n respectively.

half angle of the air bubble, and h_y is the distance of the air bubble from the free surface.

The cavitation frequency is calculated as 157 Hz in the uncoated tank under 0.87 ω/ω_n excitation. Severe structural deformations can be expected based on the wet frequency of the structure, which exceeds the scope of this study. On the other side, cavity frequency is not an issue in the hydrophobic case since there is not much visible air cavity. Fig. 11 compares the uncoated and hydrophobic coated cases under 0.65 ω/ω_n excitation in the high filling level. The free surface elevation shows not much difference with slightly calm motion due to less energy transfer per unit water i.e. less tangential velocity. When the tank is excited at a higher frequency at 0.76 ω/ω_n, the plunging breaker wave propagates toward the sidewall, but collapses and loses its current shape as it advances (Fig. 12). The wave crest overturns quickly much before hitting the sidewall in the uncoated case. However, the wave crest survives longer in the hydrophobic case, then collapses at the later stages due to increased elevation and higher velocity resulted from the reduced drag and slippage on the walls under hydrophobic effects. As seen in Fig. 12, the onset of excited water steepens higher and the impinging of the water crest is weaker under hydrophobic effects.

In order to compare the amount of water in two identical vertical halves in Figs. 9-10-12, the amount of water in both halves for a single cycle are measured via an image processing software and their ratio are plotted against time in Fig. 13. Hydrophobicity plays different role depending on the filling level. In the low filling level (Fig. 13a), there are more water accumulated on the run-up side (left half) in the hydrophobic case at the beginning of the cycle. When the bulk water moves to the right, more water translates to the right and less water remains on the left half in the hydrophobic case, so that the ratio gets larger than the one in the uncoated case. Whereas in the medium filling level (Fig. 13b), almost the same amount of water is accumulated on the run-up side (left half) in both cases at the beginning of the cycle. As the bulk water moves to the right, more water is accumulated on the right half and less water remains on the left half in the hydrophobic case. Similarly in the high filling level, hydrophobicity causes faster water transfer to the other side of the tank (Fig. 13c). This indicates that hydrophobicity promotes wave elevations due to reduced drag and slippage.

3.4. The effect of hydrophobicity on the impact pressure

Free surface deformations have major effects on hydrodynamic loads in tanks during sloshing. Hydrodynamic loads can be estimated using the linear theory and the equation $\rho g(h + H)$, where H is the wave crest elevation for a non-steep wave [24]. Fig. 11 presents this type of wave impact i.e. similar non-steep wave crest elevation in both uncoated and hydrophobic cases. Therefore, hydrodynamic loads are expected to be at the same level. However, impact histories seen in Figs. 9, 10 and 12 may result in different hydrodynamic loadings that can be measured in pressure time histories. Although the excitation signal is sinusoidal, the measured pressure signal on the side wall is not, and the peak values are random.

Pressure values obtained at each pressure sensor location on the sidewall are associated with the wave propagation. Due to the alterations in the formation and evolution of the free surface elevation under hydrophobic effects, impact pressure characteristics are different in the hydrophobic case. Lower peak pressure values are obtained at the SWL

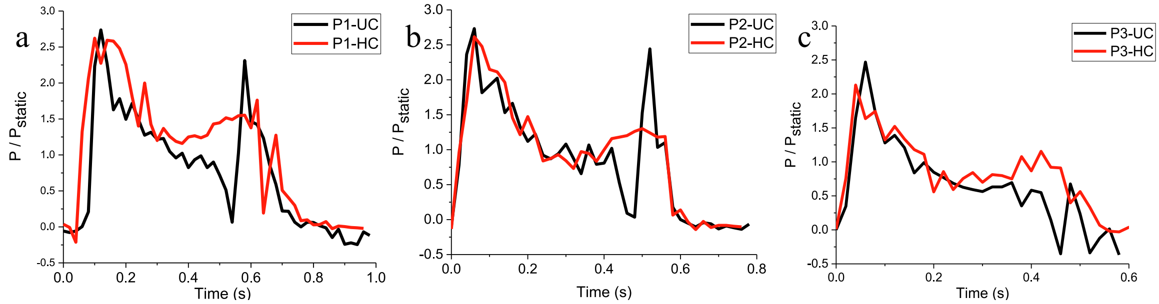

Fig. 14. Pressure-time histories obtained in the high filling level at 1.02 ω/ω_n.

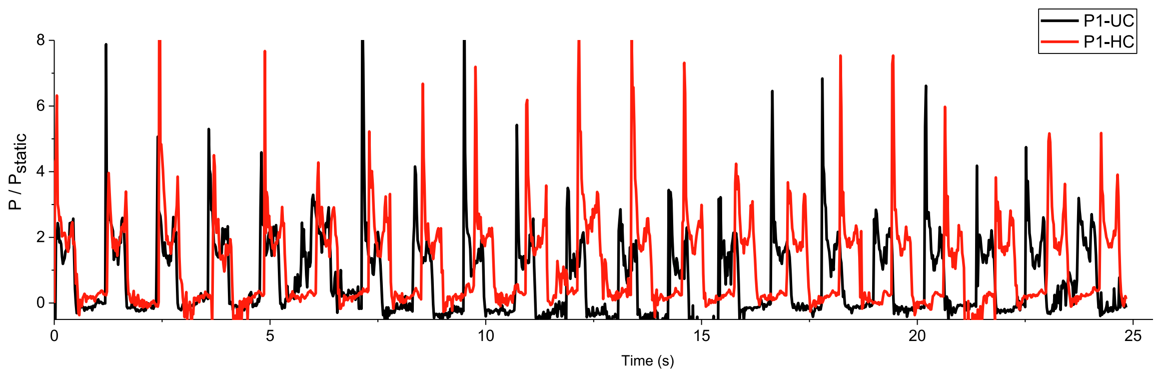

Fig. 15. Pressure-time history at P1 in the low filling level at 1.17 ω/ω_n.

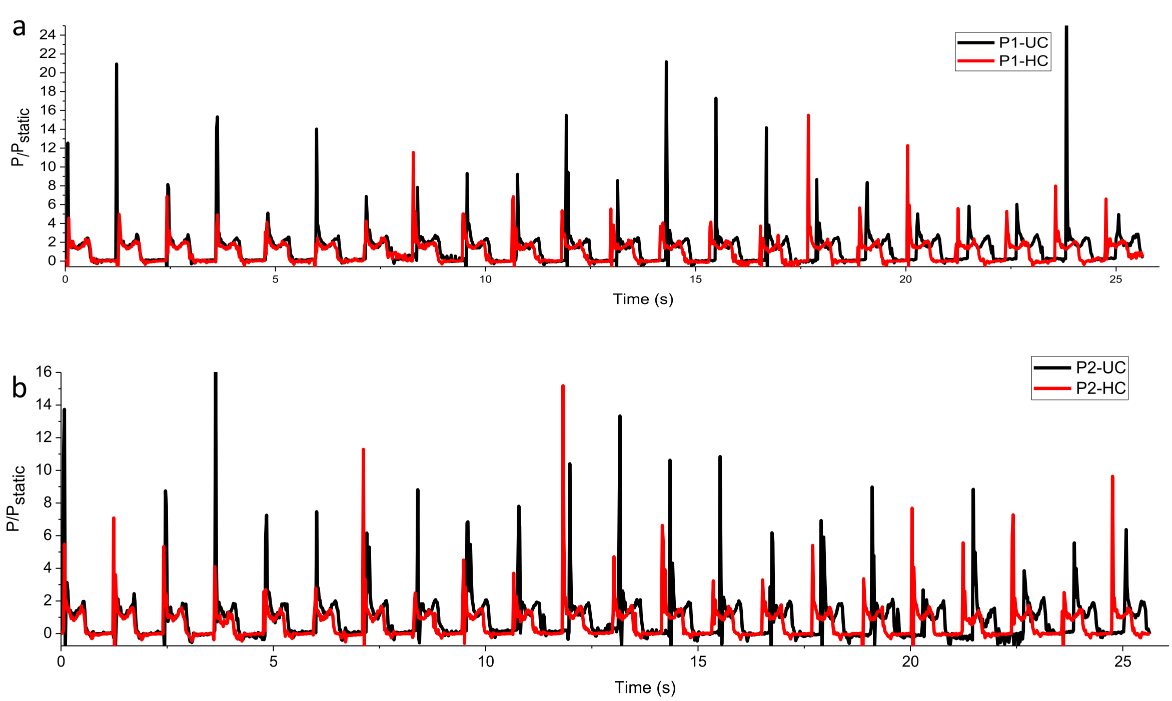

Fig. 16. Pressure-time history at P1[a] and P2[b] in the medium filling level at 0.95 ω/ω_n.

and below the SWL (P1, P2) in the hydrophobic case. Drag is reduced and the flow kinematics are altered when hydrophobicity is present (Fig. 13b). The reason for a lower peak pressure may be due to the collision being more elastic and/or having less air bubbles in the hydrophobic case (Fig. 10 at 316 ms and 348 ms, horizontal red line is at P2). This indicates that an interesting suppression effect on impact loads could be achieved by hydrophobicity, although the free surface elevations are increased and ahead of the ones in the uncoated case in phase (Fig. 13). This reduction is expected to be less significant in the high filling levels.

Fig. 14 compares the pressure–time histories of a single cycle for the uncoated and hydrophobic coated tanks in the high filling level under 1.02 ω/ω_n excitation. Under near-resonance excitation, there exists two peaks of pressure at the P1 and P2 levels in the uncoated case only. As

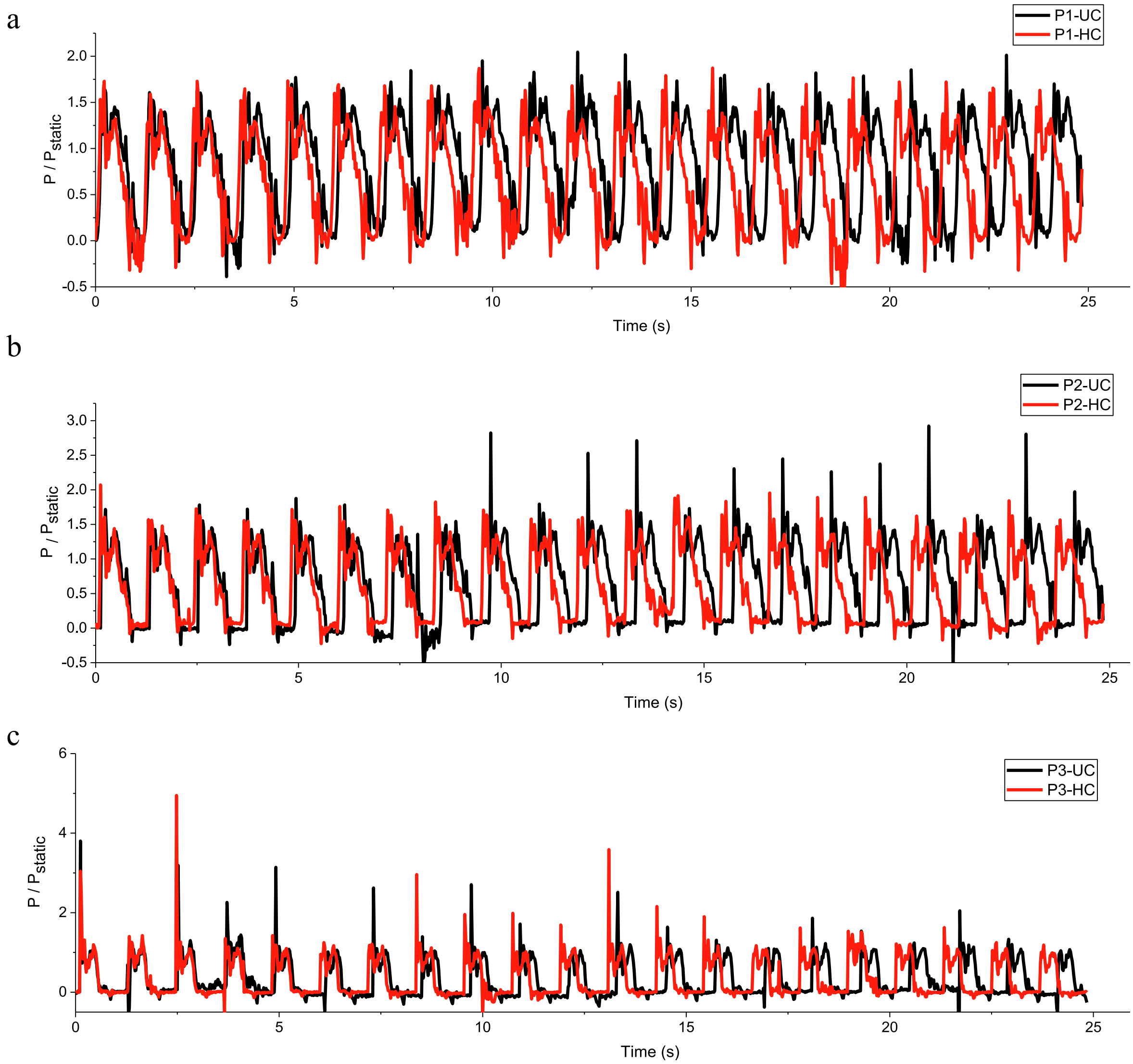

Fig. 17. Pressure-time history at P1[a], P2[b], and P3[c] in the high filling level at 0.76 ω/ω_n.

stated by Peregrine et al., 2003, Zou et al., 2015, [10], the first peak corresponds to the maximal acceleration of external excitation, thus large vertical and zero horizontal velocity due to wave run-up. The second peak is due to receding water towards down. Although the second peak is not observed in the hydrophobic case, due to tangential flow, hydrophobicity does not create much difference in the peak pressure values obtained at the P1 and P2 levels (Fig. 14a, b). However, larger peak pressure values are obtained at the highest measurement location (P3) in the uncoated case.

The pressure–time history at P1 in the low filling level is presented for 25 s in Fig. 15. As seen in Fig. 15, peak pressure values measured in a sloshing event exhibit considerable randomness. In the low filling level, a phase shift in the pressure history is observed after the third cycle in the hydrophobic case i.e. there is a delay in cycles due to larger amount of water transferred to the sides (Fig. 9, Fig. 13a) in the hydrophobic case. However, this phenomenon is different at higher filling levels (Figs. 16-17) i.e. pressure is shifted by around 0.4–0.5 s in the opposite direction in the hydrophobic case i.e. cycles are ahead in the hydrophobic case. This characteristic is also observed in Figs. 10 and 11 due to faster energy transfer in the hydrophobic case.

The average peak pressure values in both cases (UC, HC) in all filling levels are plotted with respect to the excitation frequencies (0.4 to 1.5 ω/ω_n) in Fig. 18. It can be observed in Fig. 18b that hydrophobicity decreases significantly the average peak magnitudes of sloshing loads in the medium filling level at near-resonance frequencies, although random peak pressure values may be interchangeably larger in both cases. Moreover, slightly smaller differences in average peak values are observed in the high filling level, especially at near-resonance frequencies (Fig. 18c), and the effect of hydrophobicity on peak pressure values may vary at different measurement locations. However, in the low filling level, hydrophobicity does not create much differences in peak values (Fig. 18a). Fig. 18 also shows that the resonant frequencies are not shifted under hydrophobic effects.

4. Conclusions

In the present study, an experimental investigation have been carried out to explore and characterize the effects of hydrophobicity in liquid sloshing. Experiments have been performed in a rectangular tank under various sway excitations and filling levels. The hydrophobic coated surfaces exhibited strong superhydrophobicity with the contact angles varying between 148° and 160°. Based on the comparison of the free surface profiles and the pressure–time histories obtained, it is shown that free surface elevations, wave run-ups and magnitude and characteristics of sloshing induced pressures are significantly altered when hydrophobicity is present, especially at near-resonance frequencies. The

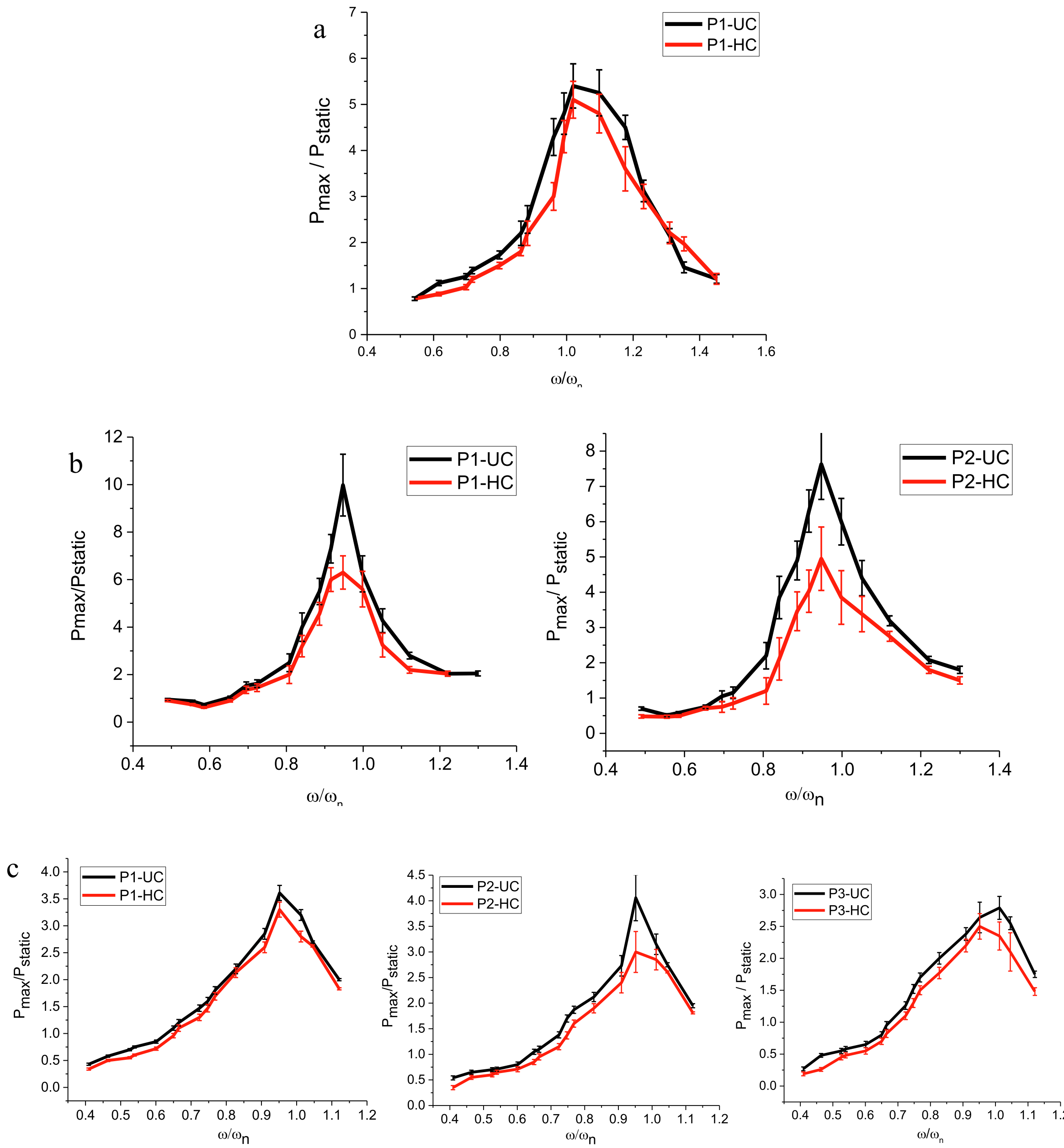

Fig. 18. Peak pressure values vs. excitation frequencies in the low [a], medium [b] and high [c] filling levels.

main conclusions drawn from the findings of this experimental study are as follows:

Due to its reduced drag and slippage effect on solid walls, hydrophobicity increases the free surface elevations and the wave run-ups along the side walls resulting in more and faster water transfer to the other side of the tank. This may negatively affect the interaction between liquid sloshing in ship tanks and ship motion.

Resulting in an elastic collision, hydrophobicity causes reduction in the impact pressures, therefore have strong sloshing suppressing effects at near-resonance frequencies without shifting the natural frequency. This reduction in sloshing loads provides improvement on the structural characteristics of liquid tanks without adding extra weights or structures e.g. baffles.

The free surface elevations and the wave propagation in the medium filling level is the strongest with higher run-ups, progressive wave breakings. Therefore, hydrophobic effects are more dominant in reducing the impact pressures e.g. no overturning of wave crests in the medium filling level.

There is no second peak observed in the pressure histories at near-resonance frequencies in the high filling level under the hydrophobic effects indicating that the impact history on the side walls is hydrodynamically and structurally different from the uncoated ones.

Violent sloshing still occurs near the theoretically determined resonance frequencies but with smaller impacts and less disturbed free surface under hydrophobic effects.

It is concluded from this study that hydrophobic surfaces cause a reduction in sloshing loads with increased free surface elevations.

CRediT authorship contribution statement

Fatih C. Korkmaz: Conceptualization, Methodology, Visualization, Writing – original draft, Writing – review & editing, Funding acquisition. **Bülent Güzel:** Conceptualization, Methodology, Writing – original draft, Writing – review & editing.

Declaration of Competing Interest

The authors declare that they have no known competing financial interests or personal relationships that could have appeared to influence the work reported in this paper.

Data availability

No data was used for the research described in the article.

Acknowledgements

This work was supported by Research Fund of the Yildiz Technical University. Project Number: FBA-2018-3341

References

[1] C.-A. Bellezi, L.-Y. Cheng, K. Nishimoto, A numerical study on sloshing mitigation by vertical floating rigid baffle, Journal of Fluids and Structures. 109 (2022), 103456.
[2] H. Bredmose, G.-N. Bullock, A.J. Hogg, Violent breaking wave impacts. Part 3. Effects of scale and aeration, J. Fluid Mech. 765 (2015) 82–113.
[3] G.-N. Bullock, C. Obhrai, D.-H. Peregrine, H. Bredmose, Violent breaking wave impacts. Part 1: Results from large-scale regular wave tests on vertical and sloping walls, Coastal Engineering. 54 (2007) 602–617.
[4] G. Cuomo, R. Piscopia, W. Allsop, Evaluation of wave impact loads on caisson breakwaters based on joint probability of impact maxima and rise times, Coastal Engineering. 58 (2011) 9–27.
[5] S. Gurusamy, V.S. Sanapala, D. Kumar, B.S.V. Patnaik, Sloshing dynamics of shallow water tanks: Modal characteristics of hydraulic jumps, J. of Fluids and Structures. 104 (2021), 103322.
[6] B. Guzel, F.C. Korkmaz, Reducing water entry impact loads on marine structures by surface modification, Brodogradnja. 71 (1) (2020) 1–18.
[7] B. Guzel, F.C. Korkmaz, Experimental investigation of water entry of bodies with constant deadrise angles under hydrophobic effects, Experiments in Fluids. 62 (2021) 107.
[8] R.A. Ibrahim, Assessment of breaking waves and liquid sloshing impact, Nonlinear Dyn. 100 (3) (2020) 1837–1925.
[9] S.C. Jiang, W. Bai, J.J. Lan, Influence of a vertical baffle on suppressing sway motion response of a tank coupled with sloshing actions in waves, Ocean Engineering 260 (2022), 111999.
[10] X. Jin, P.Z. Lin, Viscous effects on liquid sloshing under external excitations, Ocean Eng. 171 (2019) 695–707.
[11] X. Jin, M. Liu, F. Zhang, D. Li, Mitigation of liquid sloshing by multiple layers of dual horizontal baffles with equal/unequal baffle widths, Ocean Engineering 263 (2022), 112184.
[12] X. Jin, M. Luo, M.A. Xue, P. Lin, Resonant sloshing in a rectangular tank under coupled heave and surge excitations, Applied Ocean Research 121 (2022), 103076.
[13] X. Jin, J. Tang, X. Tang, S. Mi, J. Wu, M. Liu, Z. Huang, Effect of viscosity on sloshing in a rectangular tank with intermediate liquid depth, Experimental Thermal and Fluid Science. 118 (2020), 110148.
[14] M.R. Karimi, L. Brosset, J.-M. Ghidaglia, M.L. Kaminski, Effect of ullage gas on sloshing, Part I: Global effects of gas–liquid density ratio, European Journal of Mechanics - B/Fluids. 53 (2015) 213–228.
[15] Y.K. Kim, K.H. Kim, Y. Kim, Comparative study on pressure sensors for sloshing experiment, Ocean Engineering. 94 (2015) 199–212.
[16] F.C. Korkmaz, Damping of sloshing impact on bottom-layer fluid by adding a viscous top-layer fluid, Ocean Engineering. 254 (2022), 111357.
[17] F.C. Korkmaz, B. Guzel,On the effects of the number of baffles in sloshing dynamics, Ships and Offshore Structures., 18 (1) (2023) 21-33.
[18] C. Lugni, A. Bardazzi, O.M. Faltinsen, G. Graziani, Hydroelastic slamming response in the evolution of a flip-through event during shallow-liquid sloshing, Physics of Fluids 26 (2014), 032108.
[19] C. Lugni, M. Brocchini, O.-M. Faltinsen, Wave impact loads: The role of the flip-through, Physics of Fluids. 18 (2006), 122101.
[20] M. Luo, X. Wang, X. Jin, B. Yan, Three-dimensional sloshing in a scaled membrane LNG tank under combined roll and pitch excitations, Ocean Eng. 211 (2020), 107578.
[21] M. Luo, A. Khayyer, P. Lin, Particle methods in ocean and coastal engineering, Appl Ocean Res. 114 (2021), 102734.
[22] B. Molin, F. Remy, Experimental and numerical study of the sloshing motion in a rectangular tank with a perforated screen, J. Fluid Struct. 43 (2013) 463e480.
[23] H. Oumeraci, P. Klammer, H.-W. Partenscky, Classification of Breaking Wave Loads on Vertical Structures, Journal of Waterway, Port, Coastal, and Ocean Engineering. 119 (1993) 381–397.
[24] D.H. Peregrine, Water-Wave Impact on Walls, Annual Review of Fluid Mechanics. 35 (2003) 23–43.
[25] D. Peregrine, L. Thais, The effect of entrained air in violent water wave impacts, Journal of Fluid Mechanics. 325 (1996) 377–397.
[26] S.-K. Poguluri, I.-H. Cho, Analytical and numerical study of wave interaction with a vertical slotted barrier, Ships and Offshore Structures. 16 (9) (2020) 1012–1024.
[27] N. Speirs, M. Mansoor, J. Belden, T. Truscott, Water entry of spheres with various contact angles, J Fluid Mech. 862 (2019) R3.
[28] T. Sun, H. Wang, C. Shi, Z. Zong, G. Zhang, Experimental study of the effects of a viscous liquid layer on the cavity dynamics of vertical entry by a sphere into water at low Froude number, Physics of Fluids. 33 (2021), 013308.
[29] K.-P. Thiagarajan, D. Rakshit, N. Repalle, The air–water sloshing problem: Fundamental analysis and parametric studies on excitation and fill levels, Ocean Engineering. 38 (2011) 498–508.
[30] M.E. Topliss, M.J. Cooker, D.H. Peregrine, Pressure oscillations during wave impact on vertical walls, Publ by ASCE, New York, NY, United States 2 (1992) 1639–1650.
[31] Z. Wang, C. Lopez, A. Hirsa, N. Koratkar, Impact dynamics and rebound of water droplets on superhydrophobic carbon nanotube arrays, Appl Phys Lett. 91 (2007), 023105.
[32] Y. Watanabe, Y. Tsuda, A. Saruwatari, Wave packet focusing in shallow water, Coastal Engineering Journal. 62 (2020) 336–348.
[33] Z. Wei, O.M. Faltinsen, C. Lugni, Q. Yue, Sloshing-induced slamming in screenequipped rectangular tanks in shallow-water conditions, Phys. Fluids 27 (3) (2015), 032104.
[34] D.-J. Wood, D.-H. Peregrine, T. Bruce, Wave Impact on a Wall Using Pressure-Impulse Theory. I: Trapped Air, Journal of Waterway, Port, Coastal, and Ocean Engineering. 126 (2000) 182–190.
[35] W. Wu, C. Zhen, J. Lu, J. Tu, J. Zhang, Y. Yang, K. Zhu, J. Duan, Experimental study on characteristic of sloshing impact load in elastic tank with low and partial filling under rolling coupled pitching, International Journal of Naval Architecture and Ocean Engineering 12 (2020) 178–183.
[36] A.L. Yarin, Drop impact dynamics: Splashing, spreading, receding, bouncing, Annual Review of Fluid Mechanics. 38 (2006) 159–192.
[37] L. Yu, M.-A. Xue, Z. Jiang, Experimental investigation of parametric sloshing in a tank with vertical baffles, Ocean Engineering. 213 (2020), 107783.
[38] Y.-M. Yu, N. Ma, S.-M. Fan, X.-C. Gu, Experimental and numerical studies on sloshing in a membrane-type LNG tank with two floating plates, Ocean Engineering. 129 (2017) 217–227.
[39] C. Zhang, Analysis of liquid sloshing in LNG carrier with wedge-shaped tanks, Ocean Engineering. 105 (2015) 304–317.
[40] C. Zhang, P. Su, D. Ning, Hydrodynamic study of an anti-sloshing technique using floating foams, Ocean Engineering. 175 (2019) 62–70.
[41] C.F. Zou, D.Y. Wang, Z.H. Cai, et al., The effect of liquid viscosity on sloshing characteristics, J. Mar. Sci. Technol. 20 (2015) 765–775.
[42] A. Sauret, F. Boulogne, J. Cappello, E. Dressaire, H.A. Stone, Damping of liquid sloshing by foams, Physics of Fluids 27 (2015), 022103.
[43] Kortenhaus, H. Oumeraci, K.J. Mcconnell, P.J. Hewson, M. Calabrese, D. Vicinanza, H. Park, S. Engineering, P. Street, S. Road, N. IrelandWave impact loads-pressures and forcesFinal Proceedings, MAST III, PROVERBS-Project, Vol. IIa Hydrodyn. Asp (1999).
[44] D. Kisacik, P. Troch, Van Bogaert P.Description of loading conditions due to violent wave impacts on a vertical structure with an overhanging horizontal cantilever slab, Coast Eng. 60 (2012) 201–226.
[45] O.M. Faltinsen, Natural sloshing frequencies and modes in a rectangular tank with a slat-type screen, J. Sound Vib. 330 (2011) 1490–1503.